Transverse coupling of chemical waves

Vilmos Gáspár,[a] Jerzy Maselko,[b] and Kenneth Showalter
Department of Chemistry, West Virginia University, Morgantown, West Virginia 26506-6045

(Received 14 August 1991; accepted for publication 30 September 1991)

The transverse coupling of chemical waves is investigated using a model scheme for excitable media. Chemical waves supported on the surfaces of a semipermeable membrane couple via diffusion through the membrane, resulting in new types of spatiotemporal behavior. The model studies show that spontaneous wave sources may develop from interacting planar waves, giving rise to a complex sequence of patterns accessible only by perturbation. Coupled circular waves result in the spontaneous formation of spiral waves, which subsequently develop patterns in distinct domains with characteristic features. The long time entrainment behavior of coupled spiral waves reveals regions of 1:2 phase locking.

I. INTRODUCTION

Solitary chemical waves propagate in one dimension with a constant velocity and constant waveform determined by the properties of the medium.[1–4] In excitable media supporting multiple waves, interactions between the waves may result in intricate spatiotemporal patterns.[5–9] Spiral waves in 2-D and 3-D excitable media have been scrutinized in many studies and much progress has been made in unraveling the associated dynamical features.[9–16] Recently, studies have been carried out on wave behavior occurring on surfaces, such as on spherical beads[17,18] and membrane sheets.[19] In this paper, we study the transverse coupling of chemical waves in order to gain insights into chemical wave activity on the surfaces of semipermeable membranes.

We utilize a generic scheme for excitable media developed by Barkley and co-workers[20–22] to investigate cross-membrane coupling of chemical waves. The Barkley model is modified to describe an experimental system[19] in which Belousov–Zhabotinsky (BZ) chemical waves propagate on the surfaces of a Nafion (perfluorosulfonic acid) membrane loaded with ferroin catalyst. Because anions do not penetrate the resin matrix and anionic bromate is an essential reactant of the BZ reaction, wave activity is restricted to each surface of the membrane.[17,23,24] Diffusive transport of neutral species from one side of the membrane to the other results in coupling of the two chemical wave systems. New types of spatiotemporal behavior develop in this configuration including the spontaneous appearance of spiral waves and various modes of entrainment.

Our adaptation of the Barkley model to describe the membrane–chemical wave system is given in Sec. II. Cross-membrane interactions of planar waves are analyzed in Sec. III, and a mechanism for autonomous wave sources is presented. Transverse coupling of circular waves giving rise to spontaneous spiral waves is described in Sec. IV, and the subsequent entrainment behavior of coupled spiral waves is examined in Sec. V. We conclude in Sec. VI with a discussion of related work and implications of the study.

II. THE MODEL SYSTEM

We describe the Nafion–BZ system in terms of two diffusively coupled, two-dimensional chemical wave systems. The model should account for the immobilized ferroin catalyst as well as the ability of the neutral autocatalyst bromous acid to serve as a messenger species by diffusing through the membrane. We choose the Barkley model[20–22] because it mimics the fast–slow dynamics of the Belousov–Zhabotinsky reaction,[25] and it is computationally efficient. The model relies on discrete Laplacian interactions between grid points, with both time and space resolution smoothly variable. The scheme is written in terms of fast (propagator) and slow (recovery) variables u and v:

$$\frac{\partial u}{\partial t} = f(u,v) + \nabla^2 u,$$
$$\frac{\partial v}{\partial t} = g(u,v), \tag{1}$$

where the functions f and g describe the local kinetics,

$$f(u,v) = (1/\epsilon)u(1-u)[u - u_{\rm th}(v)],$$
$$g(u,v) = u - v, \tag{2}$$

and

$$u_{\rm th} = (v+b)/a.$$

Parameters a and b and the small parameter ϵ determine the local dynamics of the system. We allow diffusion of u but no diffusion of v since the catalyst is immobilized. The diffusion coefficient for u is set to unity by choosing an appropriate length scale.

The Barkley model is a good facsimile of the two-variable Tyson–Fife[25] model for the BZ reaction, with u and v corresponding to bromous acid and ferriin. For the homogeneous system without diffusion, the u nullcline is n shaped and the v nullcline linear, as shown in Fig. 1. The excitable stationary state of the system (at the nullcline crossing) is defined as the origin of the phase plane. When perturbed beyond the threshold $u_{\rm th}(v)$, the middle branch

[a] Permanent address: Dept. of Physical Chemistry, Kossuth L. University, H-4010 Debrecen, Hungary.
[b] Permanent address: Dept. of Chemistry/Physics, 3211 Providence Dr., University of Alaska, Anchorage, Alaska 99508.

 1054-1500/91/040435-10$001.00

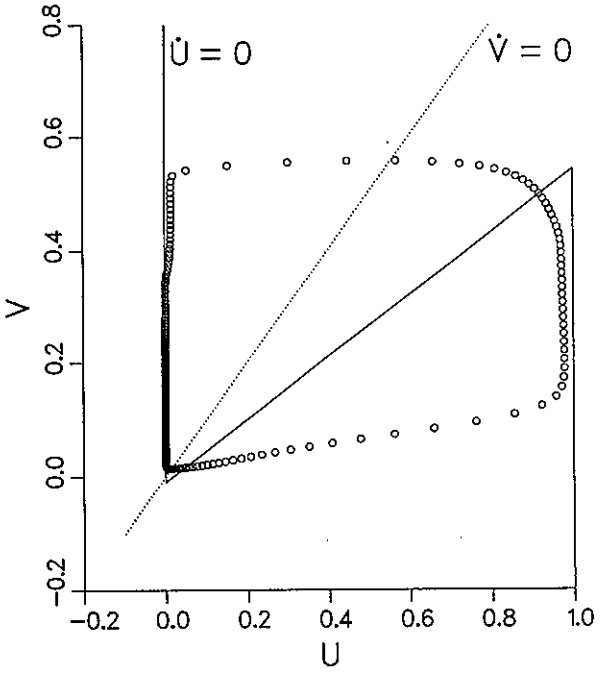

FIG. 1. Phase plane representation of Barkley model. Nullclines for the homogeneous system defined by $f(u,v)=g(u,v)=0$ in Eqs. (2) and limit cycle trajectory for spiral wave of reaction–diffusion system defined by Eqs. (1). Parameters: $a=0.55$, $b=0.01$, $\delta=1.0\times10^{-4}$, $\epsilon=0.02$, $\Delta t=0.02$. Grid is 201×201 and grid spacing is defined by $h=L/(N-1)=250/200$.

of the u nullcline, the system moves rapidly toward the right-hand branch ($u=1$) and then slowly upward. On approaching the knee, the system moves rapidly toward the other slow manifold ($u=0$) and then slowly downward toward the stationary state. The reaction–diffusion system, Eqs. (1), may also exhibit oscillatory behavior; e.g., periodic oscillations in time and space occur in a medium filled with spiral waves. The limit cycle trajectory in Fig. 1 shows an example of the temporal behavior of Eqs. (1), as a spiral wave passes through a single grid point.

The values of u and v are updated each iteration according to

$$u^{n+1}=F(u^n,u^n_{\rm th}),$$
$$v^{n+1}=v^n+\Delta t(u^n-v^n), \tag{3}$$
$$u^n_{\rm th}(v)=(v^n+b)/a,$$

where u^n and v^n are the values after the nth time step Δt. We choose an explicit Euler form for F to time step u within the excitable region:

$$F(u^n,u^n_{\rm th})=u^n+(\Delta t/\epsilon)u^n(1-u^n)(u^n-u^n_{\rm th}). \tag{4}$$

To enhance computational efficiency, a small boundary layer, δ, along the left-hand branch of the u nullcline is defined. Within this boundary layer, the value of u is set to zero:

$$u^{n+1}=0,$$
$$v^{n+1}=(1-\Delta t)v^n. \tag{5}$$

Each surface of the membrane is described by a square grid containing N^2 points in an L^2 area. The Laplacian operator at grid point (i,j) is approximated by a nine-point finite difference scheme:

$$\nabla^2 u_{ij}=\frac{1}{6h^2}\left[\sum_{r,s}A_{rs}u_{1+r,j+s}-20u_{ij}\right],$$
$$(r,s=-1,0,1), \tag{6}$$

where $h=L/(N-1)$ is the grid spacing, and the value of weighting factor A_{rs} is unity for the four diagonal grid points, four for the nearest neighbors, and zero for the center point. The diffusion term is also time stepped by an explicit Euler method. Thus, for every grid point in the excitable region,

$$u^{n+1}_{ij}=F_{ij}(u^n,u^n_{\rm th})+\Delta t\nabla^2 u^n_{ij}, \tag{7}$$

and within the boundary layer,

$$u^{n+1}_{ij}=\Delta t\nabla^2 u^n_{ij}. \tag{8}$$

The Barkley model has been used to investigate spiral wave dynamics,[22] demonstrating that transitions from simple, periodic rotations to compound, quasiperiodic rotations occur via supercritical Hopf bifurcations. No entrainment bands are exhibited within the quasiperiodic oscillatory behavior, in agreement with careful experimental measurements of BZ spirals by Skinner and Swinney.[26]

For the Nafion–BZ system we write a two-dimensional grid for side α, with variables $u(\alpha)$and $v(\alpha)$, and another for side β, with variables $u(\beta)$ and $v(\beta)$. In order to describe the effects of transverse diffusion of u on $u(\alpha)^{n+1}_{ij}$, Eqs. (7) and (8) are modified by including the coupling term

$$\gamma(\Delta t/h^2)[u(\beta)^n_{ij}-u(\alpha)^n_{ij}], \tag{9}$$

where γ is the coupling constant, $u(\alpha)^n_{ij}$ is the concentration after the nth time step, and $u(\beta)^n_{ij}$ is the concentration at the opposite grid point on side β. An analogous term is added to describe the effects of transverse coupling on $u(\beta)^{n+1}_{ij}$. No-flux boundary conditions are applied for the edges of each two-dimensional grid.

This model has been used to describe wave entrainment behavior found in experimental studies of the Nafion–BZ system.[19] Spirals on the two sides of the membrane evolve from uncoupled to fully entrained, with intermediate raylike domains and broken spirals much like the behavior found in the experiments. We focus here on the transverse coupling of planar and circular waves to gain insights into the formation of self-sustaining wave sources, and we extend our studies of spiral entrainment behavior.

III. COUPLED PLANAR WAVES

The simplified behavior of effectively 1-D propagation provides insights into the basic mechanism of transverse

coupling; we therefore examine a restricted version of the model corresponding to planar waves propagating in opposite directions on each side of the membrane. A coupled double lattice of $2\times3\times101$ grid points is used to simulate a narrow strip of membrane. Waves are initiated simultaneously every 190 iterations at each end of the strip, one wave on side α and one wave on side β. The initiation frequency was chosen to be close to that of the autonomous spiral wave in the full grid. The waves are initiated by discontinuously increasing the values of u and v in the three points at each end of the grid to 0.9 and 0.1, respectively, values far beyond the excitation threshold (cf. Fig. 1).

A plot of wave position as a function of time for a system with no transverse coupling is shown in Fig. 2(a). The open and closed circles show grid points on the α and β sides, respectively, where the value of v is greater than 0.2; hence, the rise in the wave front as well as decay of the wave back is indicated. We choose to follow v because ferriin is the measurable component in the experimental system; the choice of 0.2 as the cutoff, while arbitrary, serves to distinguish between excited and excitable regions. Figure 2(a) shows the asymptotic behavior of waves initiated on the α side propagating downward and waves initiated on the β side propagating upward. At any time there are either five or six waves on the α layer and the same number on the β layer.

The effects of strong transverse coupling are shown in Fig. 2(b), calculated with the same parameters and initial conditions as Fig. 2(a) except with the coupling constant $\gamma = 0.39$. With strong coupling, waves initiated on one side of the membrane almost immediately result in the initiation of waves in the excitable medium on the other side. Thus we see entrained waves on both sides of the membrane emanating synchronously from each end, even though initiation at each end occurs on only one side. The double waves annihilate at the center of the grid, much like colliding waves in thin films of solution.

At coupling strengths between these extremes, a complex pattern of behavior emerges as the value of γ is varied. An example is shown in Fig. 3, calculated with the coupling strength $\gamma = 0.32$. We see a wave emanating from an initiation site (indicated by the upper arrow) on the α side undergoing seven crossings with waves on the β side and then giving rise to a spontaneous wave initiation on the β side. An example of a wave source on the β side is indicated by the lower arrow. The newly initiated β wave propagates downward synchronously with the α wave; however, it also propagates upward, crossing seven waves on the α side until it, too, gives rise to a spontaneous wave initiation on the α side. An important feature of this pattern is that it is self-sustaining, i.e., no external perturbations are necessary for the ongoing initiation and propagation of the waves. The pattern in Fig. 3 was calculated without any external perturbations for 8000 iterations.

An explanation of the self-replicating patterns is offered in the schematic diagrams of Fig. 4. Diagrams (a) and (b) show waves on each side of the membrane propagating in opposite directions. Because the wave front on one side coincides with the refractory period of the wave on the other side, the transverse coupling has little effect. In diagram (c), however, the orientation is such that the front on one side aligns with the excitable region on the other side, and a wave is spontaneously initiated in this region. Spontaneous initiations occur symmetrically on each side of the membrane, with waves propagating outward from each source, as shown in diagram (d). The outermost waves propagate synchronously with the parent waves on the other side of the membrane; the inner waves propagate toward each other, passing at the midpoint to

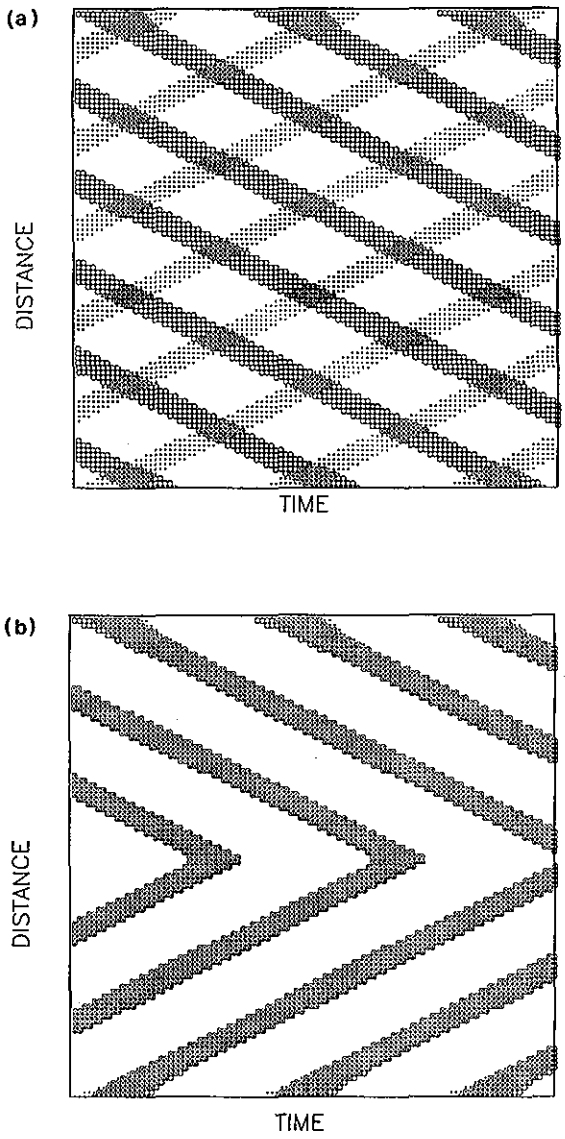

FIG. 2. Planar waves propagating on double-layered rectangular $2\times3\times101$ grid. Wave position defined by the value of v exceeding 0.2 shown by open circles for α layer and filled circles for β layer. Waves on α layer initiated at top and waves on β layer initiated at bottom every 190 iterations. Time increments represent every fifth iteration of calculation. (a) Behavior after 4000 iterations in a system with no coupling between layers. (b) Behavior after 12 000 iterations in a system with the coupling constant $\gamma = 0.39$, where coupling was switched on after 4000 iterations. Parameters same as in Fig. 1 except grid spacing defined by $h=L/(N-1) = 65/100$.

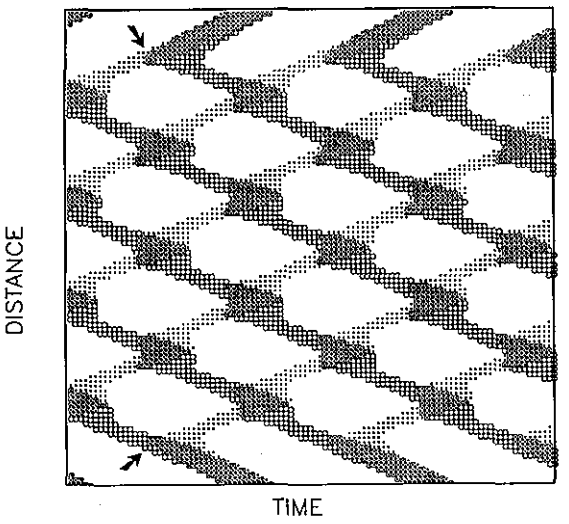

FIG. 3. Self-replicating pattern with intermediate coupling strength, $\gamma = 0.32$. Examples of wave sources on α and β layers indicated by upper and lower arrows. Calculation carried out in a sequence of steps to assure asymptotic behavior: perturbation induced waves for 4000 iterations as in Fig. 2(a), coupling between layers switched on for 8000 iterations, perturbations switched off for 8000 iterations. Wave initiation and crossing designation $I(c) = 1(7)1$. Parameters same as Fig. 2.

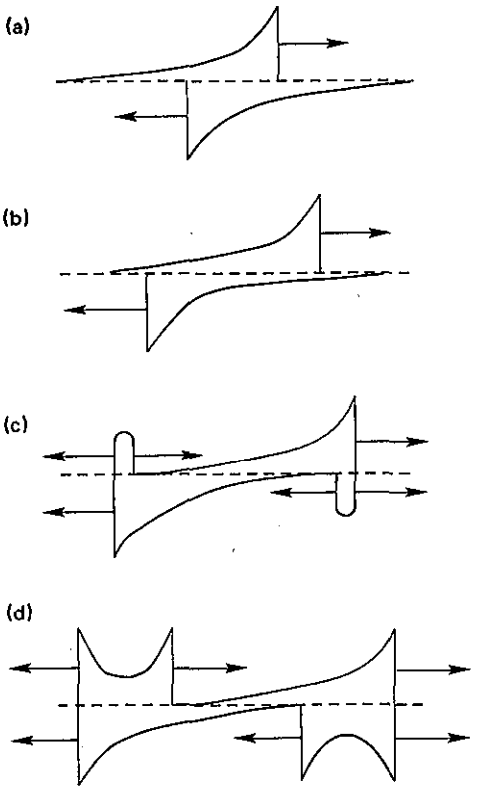

FIG. 4. Schematic representation of a model for self-sustaining patterns with coupled planar waves. Diagram (a) shows waves propagating in opposite directions on layers α and β. Wave fronts in diagrams (a) and (b) coincide with refractory periods of companion waves; in diagram (c), however, wave fronts are aligned with excitable regions and new waves are initiated in these regions. Diagram (d) shows newly initiated waves: One wave propagates outward synchronously with parent wave and the other wave propagates inward. Inward propagating waves give rise to configuration in diagram (a) and sequence repeats.

yield the configuration in diagram (a). Thus the pattern is self-replicating, with each spontaneously initiated wave giving rise to a spontaneous initiation on the other side of the membrane. The pattern shown schematically in Fig. 4 can now be recognized in Fig. 3: Two waves are generated at each wave source on the α and β sides. One wave propagates outward together with the parent wave; the other propagates inward, crossing with seven waves before serving as a parent of a new wave source. The patterns in Figs. 3 and 4 are the same except that there are seven wave crossings in the former and only one in the latter. In fact, the number of crossings varies with coupling strength and this dependence gives rise to a complex array of patterns.

Many different patterns are exhibited in the coupled planar wave configuration; it is therefore necessary to devise an identification scheme in describing the behavior. We shall use a scheme that simply identifies the number of wave sources or initiation sites and the number of wave crossings. Thus, in Fig. 3, the initiation-crossing number $I(c) = 1(7)1$ since there are seven crossings between the wave source and where the wave initiates another source on the other side. Only self-sustaining patterns are identified; patterns that rely on external perturbations, e.g., those in Fig. 2, are not included in the scheme.

Figure 5 shows the various $I(c)$ patterns exhibited as the coupling parameter γ is varied. The most striking feature is that the self-sustaining patterns occur in an apparent isola, i.e., they are accessible only by perturbing the system from the homogeneous steady state. The diagram was determined by first calculating the perturbation-dependent pattern in Fig. 2(a). The calculation was carried out until asymptotically stable behavior was exhibited at 4000 iterations; coupling was then switched on with $\gamma = 0.32$. Asymptotically stable behavior was obtained in the coupled system after 12 000 iterations, at which time the perturbations were switched off. The self-sustained pattern is much the same as the coupled pattern with perturbations, as the waves initiated by the perturbations are annihilated by those from the spontaneous sources near each end of the

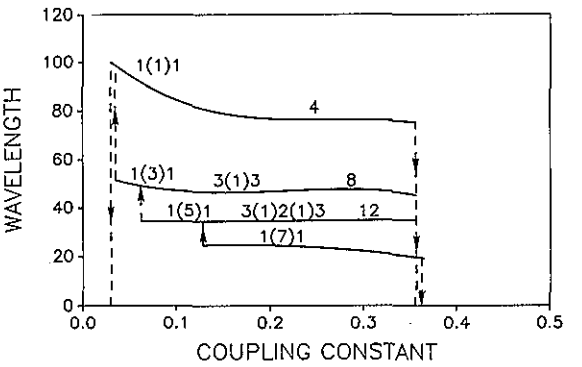

FIG. 5. Average wavelength as a function of coupling strength. Four branches of patterns occur in isola. Pattern identification scheme explained in text.

grid. In a long duration test of stability, the self-sustaining 1(7)1 pattern in Fig. 3 remained unchanged for 50 000 iterations.

Little change in the 1(7)1 pattern occurs with increasing γ until, at about 0.36, a qualitative change in behavior is exhibited with the system returning to the homogeneous steady state. Once in the steady state, the system remains there indefinitely (in the absence of perturbations) regardless of variations in the coupling constant. Decreasing the coupling constant from $\gamma = 0.32$ results in a more complex sequence of behavior for the 1(7)1 pattern. Little change occurs until $\gamma \approx 0.128$, where a transition to a new pattern takes place. The new self-sustaining pattern differs from its parent in that it has five crossings rather than seven; the $I(c)$ designation is therefore 1(5)1. On increasing γ, the new pattern undergoes a transition to the homogeneous steady state at $\gamma \approx 0.36$; on decreasing γ, a transition to another pattern, $I(c) = 1(3)1$, occurs at $\gamma \approx 0.062$. This pattern similarly undergoes a transition at $\gamma \approx 0.36$ to the homogeneous steady state and a transition at $\gamma \approx 0.034$ to another pattern, $I(c) = 1(1)1$. This last pattern corresponds to the schematic diagram in Fig. 4, with two wave sources and one wave crossing. Increasing the value of γ again results in a transition to the homogeneous steady state at $\gamma \approx 0.36$; however, now on decreasing the value of γ, a transition returns the system to the steady state rather than to another pattern. All together, the patterns constitute a four-level isola.

Two features of the transitions in Fig. 5 merit further comment: First, although the transitions represent discontinuous changes in qualitative behavior, the transient behavior is often very long lived; second, due to long transients and the iterative nature of the calculations, the transition points are only approximately determined. The latter is especially important for the transitions at $\gamma \approx 0.36$; these transitions may all occur at the same value or there may be an unresolved sequence similar to that at low coupling strengths.

A secondary level of pattern formation is also exhibited in Fig. 5. Each pattern undergoes qualitative changes as the value of γ is increased until the transition to the homogeneous steady state occurs. The exact values of γ at which these changes occur are difficult to determine because the transitions take place smoothly, with wave crossings gradually transformed into wave sources as the coupling strength is increased. Figure 6 shows an example of the changes in behavior. The pattern $I(c) = 1(3)1$, shown in Fig. 6(a), is the result of the discontinuous transition from pattern $I(c) = 1(5)1$ at low coupling strength (cf. Fig. 5). On increasing the value of γ, this pattern undergoes a transformation to a pattern with three wave sources separated by one crossing; hence, $I(c) = 3(1)3$, as shown in Fig. 6(b). Further increasing γ gives rise to eight sources and no crossings, pattern $I(c) = 8$ shown in Fig. 6(c), which is sustained until the transition to the homogeneous steady state at $\gamma \approx 0.36$. The secondary patterns fully develop in every branch except the first, which partially exhibits the transformation of crossings to sources,

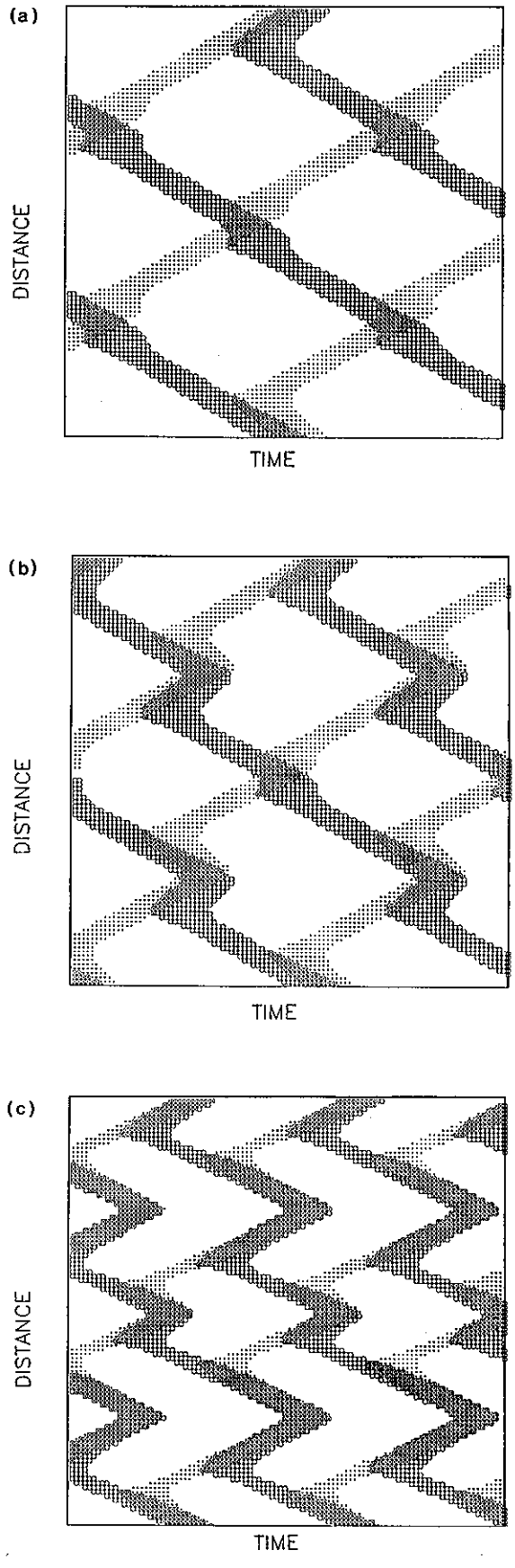

FIG. 6. Patterns of third branch of isola in Fig. 5. (a) Pattern $I(c) = 1(3)1$ at low coupling strength, $\gamma = 0.06$; (b) pattern $I(c) = 3(1)3$ at intermediate coupling strength, $\gamma = 0.10$; and (c) pattern $I(c) = 8$ at high coupling strength, $\gamma = 0.30$. Values of parameters and computational method same as Fig. 2.

but is apparently unable to develop all 16 sources that are potentially possible.

A complex array of spatiotemporal patterns arises from the transverse coupling of planar waves. We have presented a description of the possibilities when the initial perturbations are synchronous. The symmetry displayed in Fig. 5 is particularly intriguing: $I(c)$ numbers of 1(1)1, 1(3)1, 1(5)1, and 1(7)1 occur at low coupling strengths; at high coupling strengths where each wave crossing is converted into two wave sources, $I(c)$ numbers of 4, 8, 12, and (potentially) 16 are exhibited. Calculations carried out with out-of-phase perturbations show that a similar multilayered isola structure arises but with unsymmetrical patterns. We have not systematically examined the effects of grid length L, perturbation frequency, and excitation threshold defined by parameters a and b, all of which may play a role in the overall behavior.

IV. COUPLED CIRCULAR WAVES

One of the most striking features of the Nafion–BZ experiments is the spontaneous appearance of spiral waves. Although some of the spirals appear to be the result of imperfections of the experiment such as stirring induced anisotropy, there is compelling evidence that some arise from the transverse coupling of waves in target patterns early in the course of the experiment. In this section, we focus on spiral waves arising from cross-membrane coupling.

Two experimental observations[19] are of key importance in modeling the spontaneous spiral formation: (a) target patterns exhibited early in the experiment are replaced by counterrotating spirals appearing at wave crossing sites, and (b) small differences in wavelength are exhibited in spiral waves on each side of the membrane. The latter is apparently due to small nonuniformities in stirring efficiency; wavelength differences can also be deliberately induced by separating two different reaction mixtures with the membrane. Therefore, to simulate the experimental behavior, we utilize a coupled double lattice comprised of $2\times201\times201$ grid points with differing kinetic parameters in each layer. We choose to induce a relatively large difference by setting the parameter b in Eq. (2) to 0.010 and 0.0305 in the α and β layers, respectively. These values give rise to spiral frequencies differing by about a factor of 2 in the layers.

Initial conditions were chosen in an effort to mimic the experiment, with a target pattern initiated in the β layer by applying a perturbation ($u=0.9$, $v=0.1$) in a 3×3 square of grid points every 500 iterations. The transverse coupling is maintained constant ($\gamma=0.2$) throughout the calculation. Figure 7(a) and (b) shows the resulting target pattern and a cross section of the grid giving the concentration profile of v after 1250 iterations. Due to the relatively strong transverse coupling, a target pattern also develops in the α layer, almost completely synchronized with that in the β layer.

As described in Sec. II, spontaneous wave sources may develop when coupled waves propagating in opposite directions interact. We therefore deliberately initiate a single

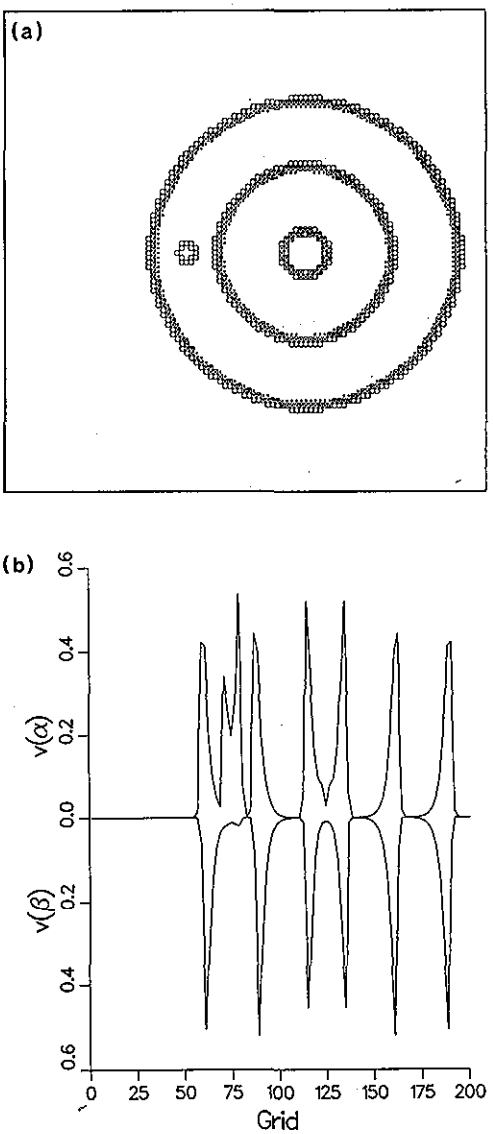

FIG. 7. (a) Perturbation initiated target pattern on coupled double lattice of $2\times201\times201$ grid points after 1250 iterations. Wave position defined by the value of v exceeding 0.3 shown by open circles for α layer and filled circles for β layer. Parameter b is 0.010 and 0.0305 on α and β layers, respectively, and transverse coupling constant $\gamma=0.2$. Other parameters same as Fig. 1. Target pattern is initiated on β layer by applying perturbation to 3×3 grid of points every 500 iterations. Second circular wave initiated on α layer by applying perturbation to 3×3 grid of points after 1150 iterations. (b) Cross section of grid (cut at $j=99$) showing concentration profile of v on the two layers.

wave on the α layer by applying a perturbation in a 3×3 grid of points after 1150 iterations. This perturbation gives rise to a circular wave on the α layer, which can be seen in Fig. 7(a) and which appears in the v concentration profile in Fig. 7(b). The newly initiated wave propagates out radially on the α layer and, when it collides with another α wave arising from the original source, annihilation occurs, as shown in Fig. 8(a). The corresponding wave on the β layer is little affected, however.

The differing values of the parameter b in the α and β layers result in differing excitabilities and refractory periods in each layer: The threshold for excitation in the β

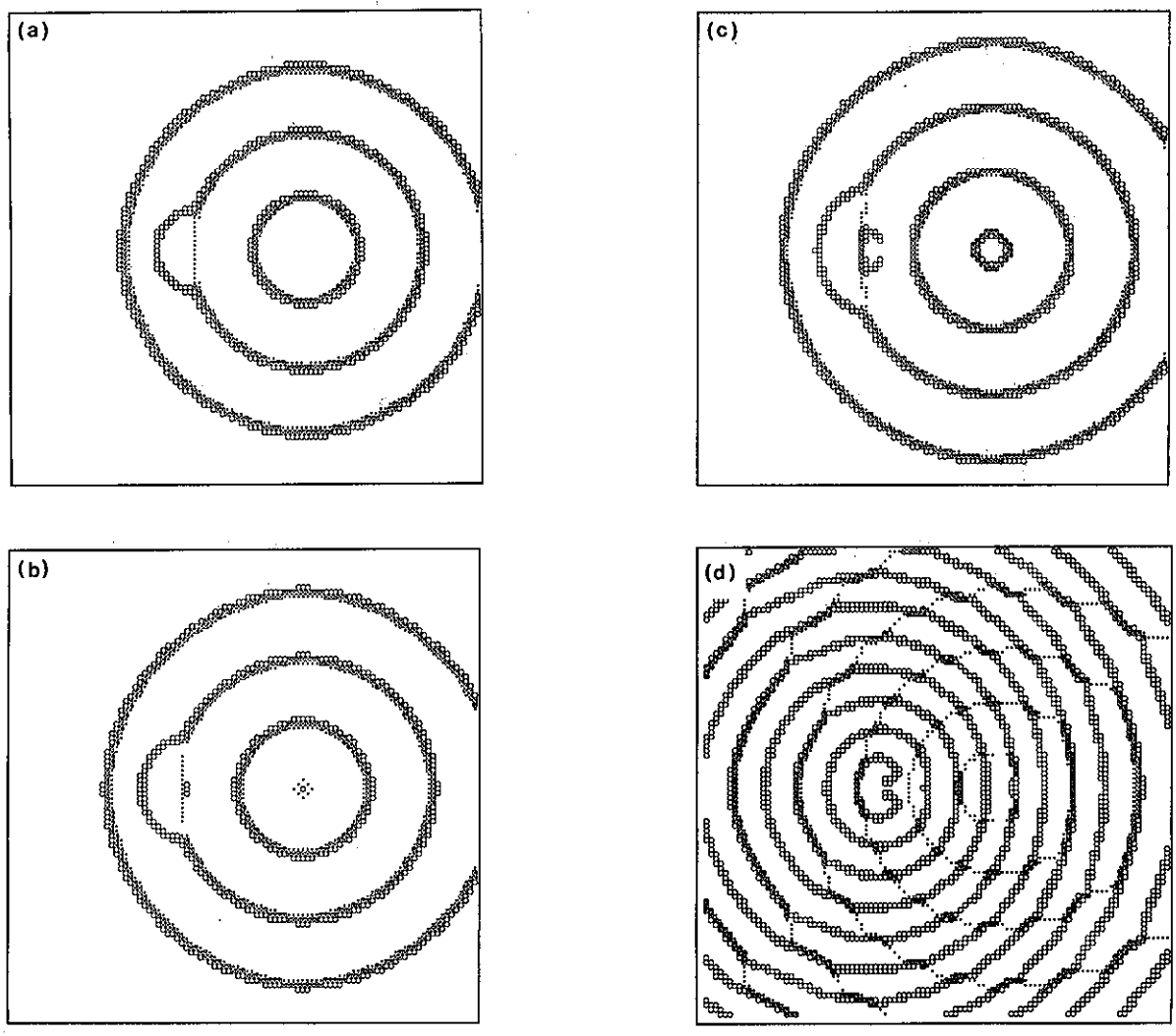

FIG. 8. (a) Collision of newly initiated wave on α layer with another α wave arising from original source after 1500 iterations. (b) Remaining β wave gives rise to initiation of new wave on α layer after 1600 iterations. (c) New α wave evolves into counterrotating spirals after 1700 iterations. (d) Behavior after 5900 iterations showing additional effects of transverse coupling: regions of entrainment, 1:2 phase locking, and stairstep regions similar to those found in Nafion–BZ experiments.

layer is greater than that in the α layer. This arrangement leads to the initiation of a wave on the α layer by the β wave remnant, shown in Fig. 8(b). The α wave fragment evolves into counterrotating spirals, as shown in Fig. 8(c), governed by the combined excitability and recovery properties of the two layers.

The general features of the newly initiated counterrotating spirals remain much the same for many iterations. Figure 8(d) shows the behavior after 5900 iterations. The spiral rotors are sufficiently close to each other that they give rise to nearly circular waves to form a target pattern. Additional effects of the transverse coupling are also evident; for example, regions of entrainment occur where the waves have a common directional component. We also see stairstep regions similar to the patterns observed in the Nafion–BZ experiments. In regions of entrainment, 1:2 phase locking is exhibited, reflecting the inherent differences of the layers. Figure 9 shows the counterrotating spirals after 6150 iterations (top), enlarged and reoriented, for comparison with spiral waves appearing at wave crossings in the Nafion–BZ system (bottom).

Figure 10 shows the pattern after 24 750 iterations. The counterrotating spirals have moved apart and are more fully developed, much like the experimental patterns. The drift of the spiral rotors is apparently due to the transverse diffusion from the perturbation-generated target pattern on the β layer. Partial entrainment in a 1:2 fashion occurs where the waves have a common directional component. In an experimental setting, the pacemaker of the target pattern would likely be influenced and possibly annihilated by the spiral waves, a factor not taken into account by the calculations.

V. COUPLED SPIRAL WAVES

Following the appearance of spiral waves, the transverse coupling gives rise to a complex sequence of transient behavior, ultimately leading to some form of spatiotempo-

ral entrainment. Previous modeling studies[19] have shown several factors to be of importance in the entrainment behavior: The coupling strength γ plays a critical role in the duration and nature of the transient behavior and in the final form of the entrainment; also important are the rotational periods of the autonomous spirals on each side of the membrane. The latter is dramatically illustrated in calculations with coupled spirals that have equal rotational periods; entrainment occurs but in broken waves with spatial incoherence unlike that seen in experiment. Behavior like that found in experiment is dependent on there being some difference in the rotational periods of the coupled spirals.

Figure 11(a) shows uncoupled spirals with rotational periods in an approximately 1:2 ratio (actual ratio 246:471), where the higher frequency spiral is on the α side of the membrane. The stable uncoupled system (after 7000 iterations) was used as the initial conditions in subsequent calculations of coupled waves. Figure 11(b) shows the behavior with coupling switched on ($\gamma = 0.4$) for 300 iterations. Although the ghost of the lower frequency spiral on the β side is still discernible, the overall behavior is dominated by the higher frequency spiral on the α side. Essentially all of the β wave segments are entrained by the α spiral at this stage; however, there is a complicated sequence of patterns before the final asymptotic behavior is exhibited at about 4000 iterations. Figure 11(c) shows an example of the stable behavior after 24 000 iterations. We see that wave activity near the spiral core occurs only on the α side, a feature discussed in more detail below. We also see 1:1 and 1:2 regions of entrained behavior. These regions tend to drift over time; however, the overall qualitative features of the pattern remain the same. The first segment of entrained β wave near the core results from a spontaneous periodic initiation that grows while moving outward; the overall pattern is dependent on the appearance of this first segment.

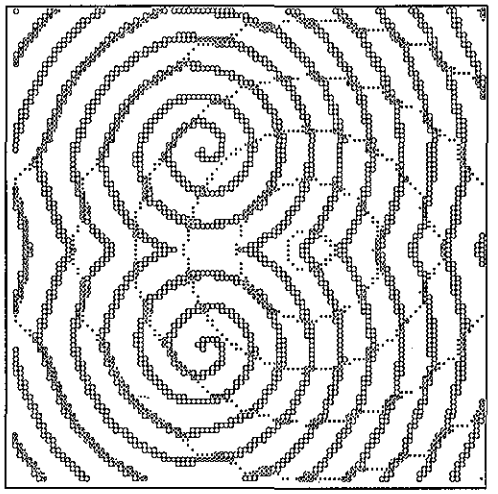

FIG. 10. Behavior of counterrotating spirals in Fig. 8 after 24 750 iterations.

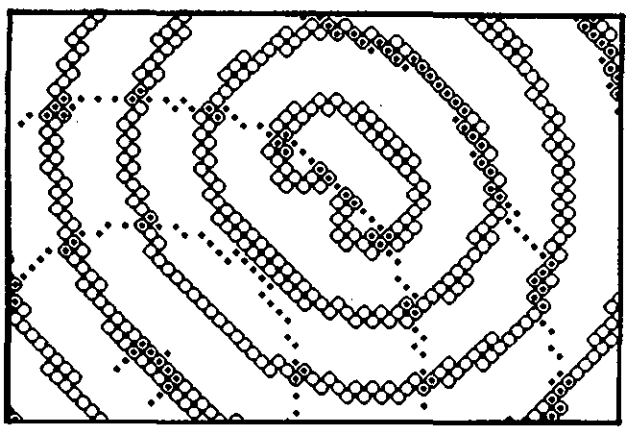

FIG. 9. Enlarged and reoriented counterrotating spirals in Fig. 8 after 6150 iterations (top). Spirals appearing at wave crossings in Nafion–BZ system (bottom); see Ref. 19 for experimental details.

An enlargement of the spiral core region at 12 000 iterations is shown in Fig. 12(a); the corresponding concentration profile of ν on the β side is shown in Fig. 12(b). The inability of the β wave to entrain near the core is of special interest. As the coupling strength is decreased, this region grows, eventually taking over the entire lattice of the calculation. Although a larger grid might reveal the presence of entrained β waves farther out from the core, it is likely that there is a critical value of γ at which wave activity on the β side is completely suppressed. This behavior is reminiscent of phase death[27] observed in coupled CSTRs; however, because our grid size is limited, we are unable to determine a critical coupling strength for the behavior. The coupling strength plays another role in determining the final stable behavior: As shown in our earlier study,[19] high values of γ tend to lock entrained waves into broken segments, which do not give way to any particular organizing center. Apparently, the spiral character of each broken segment is determined by an average of the properties of the two layers, and therefore no spiral becomes dominant. We have also found that regions of 1:2 behavior interspersed in 1:1 behavior, as in Fig. 12, are exhibited regardless of the autonomous spiral frequencies. Thus we have been unable to find distinct regions of 1:3 behavior in systems with spiral frequencies differing by a factor of 3.

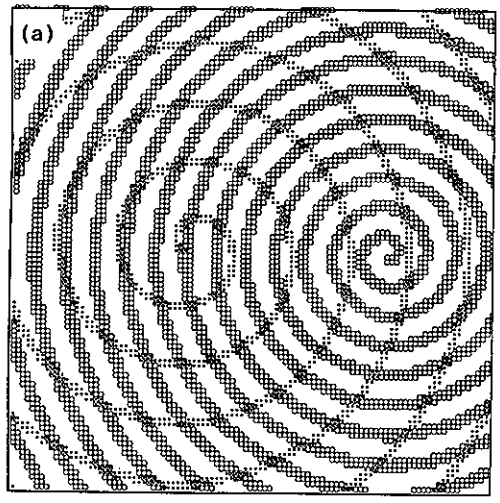

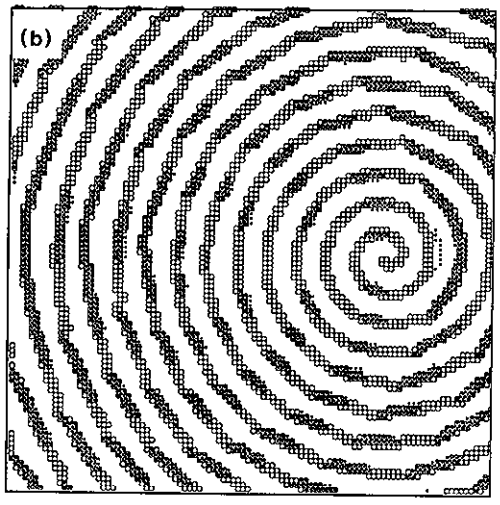

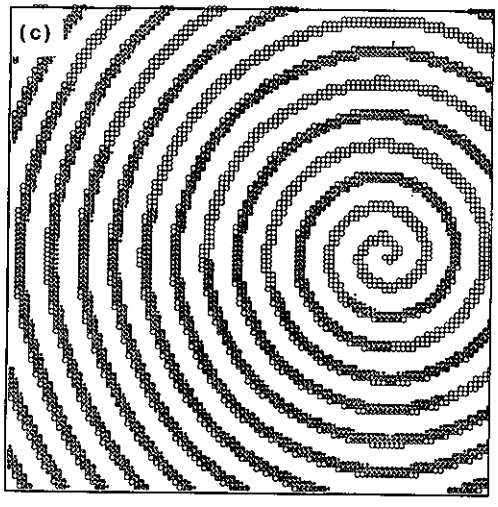

FIG. 11. Spiral waves propagating on double-layered $2\times201\times201$ grid. (a) Uncoupled spirals on α and β sides shown by open and filled circles after 7000 iterations; wave position defined by the value of v exceeding 0.2. Period of autonomous spirals in α and β layers 246 and 471 iterations, respectively. (b) Behavior after 300 iterations with $\gamma = 0.4$ showing regions of partial entrainment. (c) Behavior after 24 000 iterations with $\gamma = 0.4$. Parameters same as Fig. 1.

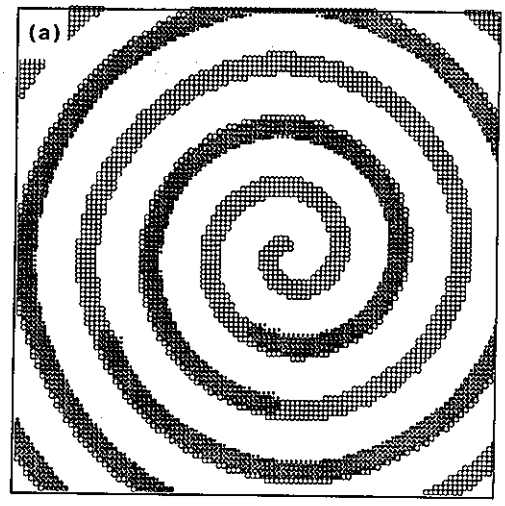

(b)

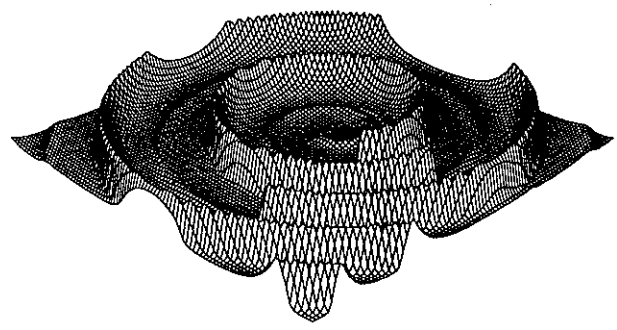

FIG. 12. (a) Enlarged region of Fig. 11 at 12 000 iterations with $\gamma = 0.4$. (b) Concentration profile of v on β layer showing shadow of spiral core on α layer and segments of entrained β waves.

VI. CONCLUSION

Transverse coupling of chemical waves gives rise to a rich variety of reaction–diffusion behavior, including spontaneous spiral formation and entrainment of one set of waves by another. The self-sustaining patterns arising from coupled planar waves represent a new type of autonomous wave source, analogous to spiral and scroll waves in two- and three-dimensional excitable media. The development of counterrotating spirals from coupled circular waves provides insights into similar behavior found in Nafion–BZ experiments and may represent a mechanism for the origin of spiral wave activity in biological systems. The spiral formation is reminiscent of Winfree's[28] spatially graded stimulus experiment for initiating counterrotating spirals. The subsequent interaction of spiral waves leading to various forms of entrainment may provide insights into cross-membrane communication in biological systems. It seems plausible that calcium waves on the surfaces of newly fertilized cells[29] might affect the calcium cycle[30] in the cell interior via cross-membrane communication.

Our modeling of coupled chemical waves has focused on developing insights into the Nafion–BZ system; however, this study is also relevant to other recent experimen-

tal investigations. Zhabotinsky, Müller, and Hess[31] have studied layers of chromatographic silica gel saturated with BZ reagent. The inhibiting effect of oxygen on the reaction gives rise to two weakly coupled chemical wave systems: a highly excitable, oxygen poor lower layer and a less excitable, oxygen rich upper layer. The two layers are diffusively coupled and stairstep behavior much like that found in the Nafion–BZ system is observed. Another study by Linde and Engle,[32] based on a similar experimental configuration, examined spontaneous counterrotating spirals arising from the interlayer coupling. Studies of coupled wave systems might offer insights into the origin of certain types of spiral wave activity in myocardium tissue.

ACKNOWLEDGMENTS

We thank the National Science Foundation (Grants CHE-8920664 and INT-8822786) for financial support of this work. We also thank Dr. Dwight Barkley of Princeton University for many enlightening discussions.

[1] R. Luther, Z. Elektrochem. **12**, 596 (1906); R. Arnold, K. Showalter, and J. J. Tyson, J. Chem. Ed. **64**, 740 (1987); K. Showalter and J. J. Tyson, J. Chem. Ed. **64**, 742 (1987).
[2] R. A. Fisher, Ann. Eugenics **7**, 355 (1937).
[3] A. Saul and K. Showalter in *Oscillations and Traveling Waves in Chemical Systems*, edited by R. J. Field and M. Burger (Wiley, New York, 1985), pp. 419–439.
[4] P. Gray, S. K. Scott, and K. Showalter, Philos. Trans. R. Soc. London (in press).
[5] A. N. Zaikin and A. M. Zhabotinsky, Nature **225**, 535 (1970).
[6] A. T. Winfree, Science **181**, 937 (1973).
[7] J. J. Tyson and J. Keener, Physica D **32**, 327 (1988).
[8] J. Ross, S. C. Müller, and C. Vidal, Science **240**, 469 (1988).
[9] A. T. Winfree, *The Geometry of Biological Time* (Springer-Verlag, New York, 1984).
[10] Z. Nagy-Ungvarai, S. C. Müller, J. J. Tyson, and B. Hess, J. Phys. Chem. **93**, 2760 (1989).
[11] J. Keener and J. J. Tyson, Physica D **21**, 307 (1986).
[12] W. Jahnke, W. E. Skaggs, and A. T. Winfree, J. Phys. Chem. **93**, 740 (1989).
[13] A. T. Winfree and W. Jahnke, J. Phys. Chem. **93**, 2823 (1989).
[14] J. Keener and J. J. Tyson, Science **239**, 1284 (1988).
[15] B. J. Welsh, J. Gomatom, and A. E. Burgess, Nature **304**, 611 (1983).
[16] A. S. Mikhailov, A. V. Panfilov, and A. N. Rudenko, Phys. Lett. A **109**, 246 (1985).
[17] J. Maselko and K. Showalter, Nature **339**, 609 (1989).
[18] J. Maselko and K. Showalter, React Kinet. Catal. Lett. **42**, 263 (1990).
[19] D. Winston, M. Arora, J. Maselko, V. Gáspár, and K. Showalter, Nature **351**, 132 (1991).
[20] D. Barkley, in *Nonlinear Structures in Physical Systems*, edited by L. Lam and H. C. Morris (Springer-Verlag, Berlin, 1990), p. 192.
[21] D. Barkley, Physica D **49**, 61 (1991).
[22] D. Barkley, M. Kness, and L. S. Tuckerman, Phys. Rev. A **42**, 2489 (1990).
[23] J. Maselko, J. S. Reckley, and K. Showalter, J. Phys. Chem. **93**, 2774 (1989).
[24] J. Maselko and K. Showalter, Physica D **49**, 21 (1991).
[25] J. J. Tyson and P. C. Fife, J. Chem. Phys. **73**, 2224 (1980).
[26] G. Skinner and H. L. Swinney, Physica D **48**, 1 (1991).
[27] M. F. Crowley and I. R. Epstein, J. Phys. Chem. **93**, 2496 (1989).
[28] A. T. Winfree, in *Oscillations and Traveling Waves in Chemical Systems*, edited by R. J. Field and M. Burger (Wiley, New York, 1985), pp. 441–472.
[29] L. Jaffe, Proc. Natl. Acad. Sci. USA (in press).
[30] A. Goldbetter, G. Dupont, and M. J. Berridge, Proc. Natl. Acad. Sci. USA **87**, 1461 (1990).
[31] A. M. Zhabotinsky, S. C. Müller, and B. Hess, Physica D **49**, 47 (1991).
[32] H. Linde and H. Engel, Physica D **49**, 13 (1991).